applied sciences

MDPI

Article

Path Tracking of Agricultural Vehicles Based on 4WIS–4WID Structure and Fuzzy Control

Lijun Xu, Qinhan Chen, Linlin Wang and Lijian Yao *

Key Laboratory of Agricultural Equipment for Hilly and Mountainous Areas in Southeastern China (Co-Construction by Ministry and Province), College of Optical, Mechanical and Electrical Engineering, Zhejiang A&F University, Ministry of Agriculture and Rural Affairs, Hangzhou 311300, China; zoelijun@zafu.edu.cn (L.X.); 2020604021005@stu.zafu.edu.cn (Q.C.)
* Correspondence: ljyao@zafu.edu.cn; Tel.: +86-0571-63793974

Abstract: This paper proposes a path-tracking method for agricultural vehicles based on the 4WIS-4WID structure and fuzzy control to improve the operation performance of agricultural machinery in the greenhouse. The influential model of two critical parameters, α and R, on the position correction is obtained based on the relationship analysis between the traditional pure pursuit model and the vehicle structure. Based on aiming pursuit, the relationship equation between the position deviation, lateral deviation d, and heading deviation θ is established. A two-input and two-output fuzzy controller is designed, and the lateral deviation d and heading deviation θ are the input variables. Values of α and R are obtained after fuzzification, fuzzy inference, and defuzzification, and a validated MATLAB model is used to simulate different scenarios. Results of the tests show that the steady-state error of path tracking based on fuzzy control pursuit is between 35 and 51 mm, and the stability distance is between 1661 and 3052 mm for straight path tracking in four initial states. The rectangular corners have the highest inaccuracy. The results of fuzzy control pursuit show a significant improvement in path-tracking performance that can influence vehicle navigation capability in the greenhouse.

Keywords: intelligent agricultural machinery; pure pursuit; fuzzy control; path tracking; 4WIS–4WID; position correction

Citation: Xu, L.; Chen, Q.; Wang, L.; Yao, L. Path Tracking of Agricultural Vehicles Based on 4WIS–4WID Structure and Fuzzy Control. *Appl. Sci.* **2023**, *13*, 8495. https://doi.org/10.3390/app13148495

Academic Editor: Dimitris Mourtzis

Received: 18 June 2023
Revised: 20 July 2023
Accepted: 21 July 2023
Published: 23 July 2023

1. Introduction

Path-tracking control at low speeds is one of the critical technologies of unmanned agricultural machines contributing to the quality and efficiency of machinery operations. Influenced by the structure of conventional tractors, researchers tend to pay more attention to the front wheel corner speed constraint, which influences path-tracking accuracy [1–3]. Advanced controller response using aiming pursuit is a commonly adopted path-tracking approach. However, constrained by the minimum steering radius, agricultural machines often take longer to converge to the desired path when the initial deviation is significant, limiting their application in tight facilities such as greenhouses. With the evolution of facility agriculture, the structure of agricultural robots is also innovating and breaking through. The pure pursuit algorithm proposed for the autonomous navigation of a centered articulated robot applied in a cotton field obtained 0.04 m, 0.06 m, and 0.09 m mean absolute error (MAE) through three tests [4]. Using an input map with predefined geospatial coordinates, the pure pursuit algorithm for an articulated steering vehicle platform determines the future heading direction and appropriate coordinates from the input map based on Global Positioning System coordinates and corresponding heading data. It calculates the required steering radius to achieve the looking-ahead distance [5]. A path-tracking controller for a tractor-trailer robot is designed through a purely geometric path-tracking approach [6]. Slip-free motion is achieved by controlling velocity, lateral deviation, and heading deviation. The quality of path tracking is ensured by a linear, time-invariant, decoupled controller for tracking straight or circular paths at a constant

velocity. Proportion Integration Differentiation (PID-control) and state feedback techniques can determine the gain. Path generation and the motion control of a tractor-trailer are implemented for autonomous maneuvers on the farmland and verified with an experimental trailer hooked to mobile power; at the end of each row, a reverse turn is automatically generated to connect the subsequent reference trajectory that can perform the maneuver automatically [7]. Based on an improved dual arc path planning algorithm, an autonomous path-tracking control method is proposed for a combined harvester with rear-wheel steering [8]. A dual DQN-based path-tracking method is proposed for crop-row agricultural machinery with a differential steering mechanism [9].

In addition to the machinery structures mentioned earlier, such as articulated, traction, and rear-wheel steering, agricultural machinery with four-wheel independent steering and four-wheel independent drive (4WIS–4WID) structure was studied and applied for its flexibility of steering and driving characteristics. Aiming to realize the dynamic switch of three steering modes in a four-wheel independent steering (4WIS) rescue vehicle without stopping, the steering control strategy is investigated, and the wheel steering trajectory is optimized based on two objectives: to minimize the sudden change of dynamic parameters and to minimize the energy consumption in the steering process [10].

Coordinated regulation of the vehicle's sway and deflection angles is required for smoother WIS steering. Up-to-date control techniques such as fuzzy and model predictive control have been applied to study direct deflection control [11–13]. The path-tracking controller introduced in [14] shows that four-channel autoturbation control (ADRC) could achieve performance like anti-side wind, anti-skid, and anti-rollover in path tracking of four-wheel steering (4WS) agricultural vehicles. Simulation results show that the 4WS autonomous vehicle with this controller has good anti-side wind, anti-skid, and anti-rollover performance in path tracking, even on curves with minor steering radius or low adhesion. A robust differential steering control system (DSCS) for an independent four-wheel drive (4WID) electric vehicle is investigated. The DSCS will operate the independent four-wheel drive electric vehicle using the input torque from all four wheels without Conventional Steering Mechanism (CSM) [15]. A design method for an integrated chassis controller was established for four-wheel independent steering (4WIS) with front slip angle constraint [16]. Simulation results by Car-sim software show that this integrated chassis controller can maintain lateral stability and maneuverability under the constraint without performance degradation. An adaptive control method for the four-wheel independent drive (4WID) unmanned sprayer was designed to track accuracy degradation due to the influence of side-slip in autonomous navigation of the high clearance sprayer [17]. A four-wheel independent steering drive control system was designed for wheel-type agricultural robots to address the problems of single steering, challenging adapting to the complex environment in the field, and high cost [18]. Either method is based on the assumption that the steering center of the prototype is on the lateral extension line of the vehicle center, or the steering modes such as crab walk, diagonal, and in situ steering of the 4WIS–4WID structured vehicle are artificially divided and switched. These methods inhibit the flexibility and rapidity of the 4WIS–4WID structured vehicle regarding position correction.

In this paper, based on the analysis of the relationship between the steering center and deviation correction, a tracking model of the 4WIS–4WID structure and fuzzy control is proposed to determine the position of the steering center according to the vehicle's positional state, which expands the vehicle's steering center from 1 DOF control to 2-dimensional plane, thus better improving the quality of path tracking for 4WIS–4WID agricultural machinery. The vehicle test results demonstrate that the proposed methods improve the vehicle navigation and path following of 4WIS–4WID agricultural machinery at low speed.

2. Materials and Methods

2.1. Configuration of Test Prototype

In this paper, a 4WIS–4WID vehicle prototype is used. Sizes of the prototype, including the length, width, and altitude, are 1200 mm, 700 mm, and 700 mm, respectively. The entire platform is made of 40 mm × 40 mm aluminum profiles, with an axle track of 540 mm, wheelbase of 1040 mm, and clearance of 600 mm, as illustrated in Figure 1. The prototype is driven by four-wheel motors (8 inches, 24 V) independently, and four servos (DH-03X, 120°/s, 38 N-m) are connected to the driving wheels through a coupling mechanism, controlling each driving wheel to achieve independent steering in the range of −90° to 90°. The prototype is powered by a 24 V, 20 Ah lithium battery.

Figure 1. Test prototype and test environment. 1. Motor driver, 2. Microcontroller, 3. Lithium battery, 4. Wheel motor, 5. UWB base station, 6. Mobile tag, 7. Servo, 8. Electronic gyroscope.

The wireless positioning system consisted of four ultra-wideband (UWB) base stations, and the UWB (I-UWB LPS PA) mobile tag installed at the center of the test prototype receives the UWB signals from the base stations and decodes them into the position information of the prototype vehicle. The position and orientation information of the prototype is provided by a 9-axis electronic gyroscope (WT901C), and the error of the position and orientation information is ±50 mm and ±0.1°, respectively. The STM32F103 is used as the central controller of the test prototype. It receives the position coordinates (x, y) of the prototype from the UWB mobile tag and information of the heading angle φ from the electronic gyroscope and then converts them into the lateral deviation d and heading deviation θ of the vehicle relative to the target path.

The path-tracking algorithm proposed in this paper calculates the speed v_1~v_4 and the steering angle δ_1~δ_4 of each wheel. The PWM signals the motor required to execute the speed and angle commands mentioned above are input to the motor driver (AQMD6015BLS) and the steering servo to execute the corresponding driving and steering actions to achieve path tracking. The prototype is also equipped with an ultrasonic sensor to detect obstacles and issue an alarm and an emergency brake when an obstacle reaches a dangerous distance. The system control rule is shown in Figure 2.

2.2. Path-Tracking Model Based on 4WIS–4WID Structure and Fuzzy Control

2.2.1. Relationship between Traditional Pure Tracking Model and Vehicle Structure

The traditional pure pursuit (TPP) algorithm is a pure geometric path-tracking model based on look-ahead aiming points [19]. As shown in Figure 3a, line P_1P_2 is the desired path of the farm machinery, and S is the look-ahead point on line P_1P_2. For the ordinary two-wheel steering and two-wheel drive (2WS–2WD) vehicle structure, W is the axle track, l is the wheelbase, Point O is the center of the rear axle, Point A is the projection of O on P_1P_2, AS is the look-ahead distance (LD), Point G is the midpoint of the look-ahead straight-line OS, and O'G is the vertical bisector of OS. The length of line OA is the lateral

deviation d, and the angle between axle OB and P_1P_2 is the heading deviation θ. From the TPP model, the location of the steering center O' is determined by the look-ahead straight-line OS and the rear axle line OO' during the path tracking of the farm robots. According to the Ackermann steering geometry, the rear vehicle axis is perpendicular to the vehicle body. Therefore the location of point O' is determined by the look-ahead straight-line OS, that is, it has one degree of freedom (DOF). By repeatedly tracking the look-ahead points on the desired path, the prototype's location and orientation are gradually adjusted so that the lateral deviation d and the heading deviation θ converge to 0 gradually. From Figure 3a, we can also obtain that the farther the steering center O' is from the prototype vehicle (i.e., the larger the steering radius R), the smaller the front wheel steering angle is needed, and the vehicle's tendency to move forward is stronger; conversely, the closer the point O' is from the prototype, the larger the steering angle of the front wheel, and the stronger the vehicle's ability to adjust its heading behavior. We should note that when point O' is located inside the prototype vehicle, the steering angle of the front wheels will be significant, and the prototype will make a point-turn motion if the steering mechanism limitation has not been considered.

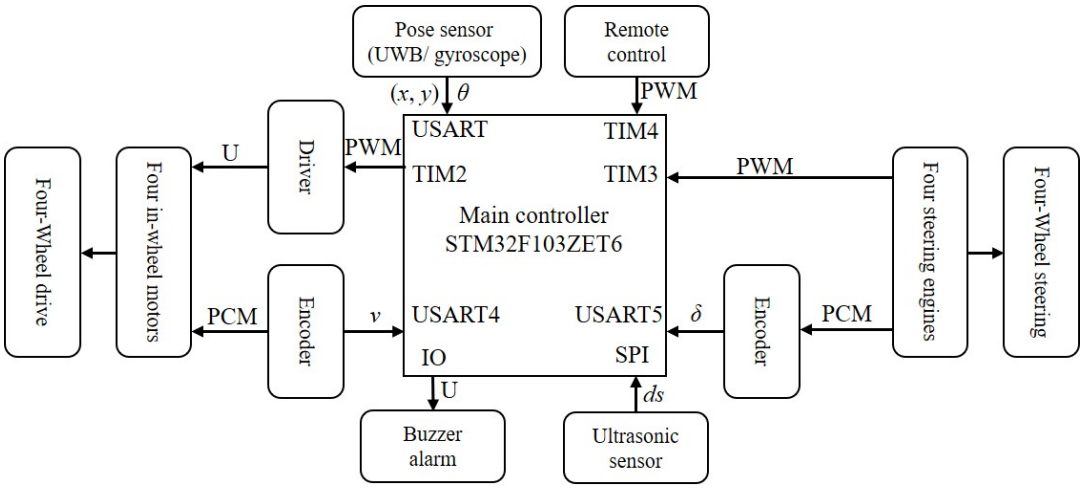

Figure 2. Schematic diagram of control system. Note: (x, y) are coordinates of mobile tag; φ is heading angle, (°); δ is steering angle, (°); v is vehicle speed, ms^{-1}; U is voltage, V; PCM means pulse code modulation; PWM means pulse code modulation; USART is universal synchronous/asynchronous receiver/transmitter; TIM is general timer; ds is distance, mm.

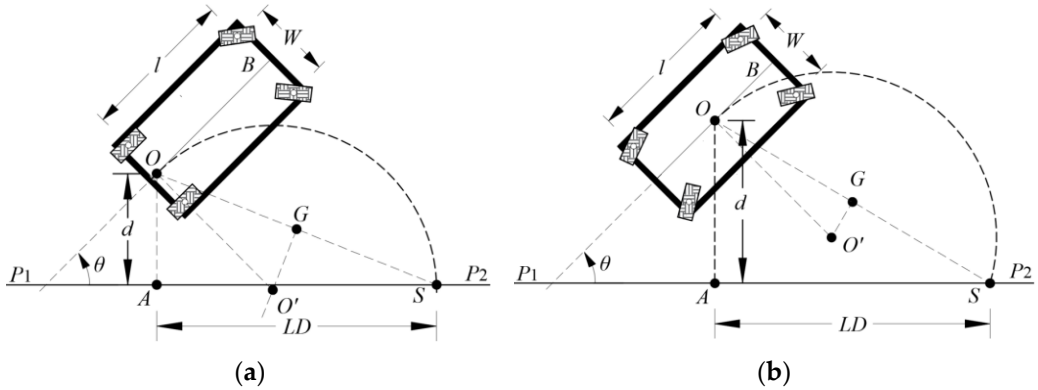

Figure 3. Traditional pure pursuit models on different structures of prototype. (**a**) 2WS–2WD, (**b**) 4WIS–4WID.

A similar control method is widely used to control the conventional 2WS–2WD structure for the test prototype with the 4WIS–4WID design (Figure 3b) [18]. The steering radius

$O'O$ consisting of the steering center O' and the gravity center O is always perpendicular to the vehicle body. The vertical foot is point O. The trajectories of the inner front and rear wheels coincide, and the same for the outer front and rear wheels. The prototype could avoid lateral movement and obtain high vehicle stability. However, the steering tends to lack flexibility. For agricultural machinery used in large farm fields or greenhouses, its transverse acceleration and lateral force can be ignored due to low speed. Therefore, the following section will mainly focus on the control rule when the steering center is randomly positioned in the prototype vehicle. The steering wheel's steering corrects the prototype's position and orientation. From the comparison (Figure 3), we can see that to obtain an equal response of steering (i.e., the same steering radius), the steering angle of each wheel of the 4WIS–4WID vehicle structures is more insignificant.

2.2.2. Influence Analysis of Steering Center Position on Vehicle Position Correction

As shown in Figure 4, provided that point O' is the steering center of the 4WIS–4WID prototype, point O is the gravity center, OO' is the steering radius R, and the angle between OO' and the vehicle axial direction (forward vehicle direction) is denoted as α. According to the Ackermann steering geometry, the following equation determines the steering angle of each wheel, namely δ_1~δ_4.

$$\begin{cases} \delta_1 = \arcsin(\frac{R\cos\alpha + l/2}{R_1}) = \arctan(\frac{R\cos\alpha + l/2}{R\sin\alpha + W/2}) \\ \delta_2 = \arcsin(\frac{R\cos\alpha + l/2}{R_2}) = \arctan(\frac{R\cos\alpha + l/2}{R\sin\alpha - W/2}) \\ \delta_3 = \arcsin(\frac{R\cos\alpha - l/2}{R_3}) = \arctan(\frac{R\cos\alpha - l/2}{R\sin\alpha - W/2}) \\ \delta_4 = \arcsin(\frac{R\cos\alpha - l/2}{R_4}) = \arctan(\frac{R\cos\alpha - l/2}{R\sin\alpha + W/2}) \end{cases} \quad (1)$$

where W is the axle track in meters, l is the wheelbase in meters. R is the steering radius at the gravity center of the prototype vehicle in meters, and the turning radius of each wheel is R_1~R_4 in meters. Then, the following equation can determine the linear velocities of each wheel.

$$\begin{cases} v_1 = v\frac{R_1}{R} \\ v_2 = v\frac{R_2}{R} \\ v_3 = v\frac{R_3}{R} \\ v_4 = v\frac{R_4}{R} \end{cases} \quad (2)$$

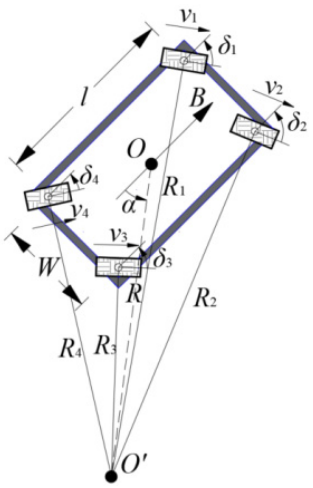

Figure 4. Steering model when the center of steering is at a random position.

In Equation (2), v is the linear velocity of the gravity center O of the test prototype and v_1~v_4 are the linear velocities of four wheels in ms^{-1}. The analysis of Equations (1) and (2) and Figure 4 leads to the following two conclusions.

1. When α is closer to 0° or 180°, steering radius R is closer to the longitudinal axis line OB, and the movement trend of the prototype vehicle tends to be the lateral crab movement. The prototype performs a quick response of lateral correction. Conversely, when α is closer to 90°, steering radius R is perpendicular to the prototype's axle, and the instantaneous movement direction is closer to the longitudinal axis line OB. The prototype performs a weak response of lateral correction.
2. The smaller the steering radius R is, the closer the steering center O' is to the gravity center O, the motion of the prototype tends to be in situ rotation, and the prototype performs more vital heading control ability. Conversely, the larger the steering radius R is, the farther the steering center O' is from the prototype gravity center O, the movement of the prototype vehicle tends to be linear motion, and the prototype performs a weak ability to control heading direction.

As discussed earlier, two variables determine the steering center O', namely, α and R. These two parameters determine the location of the steering center O' and also the control capability of the steering.

2.2.3. Discussion of the Yaw Response

Both lateral and heading deviations are amended by wheel steering. It is obvious that to achieve fast steering correction under the condition of significant variations, large steering angles of the wheels need to be adopted. As shown in Figure 5, the variables are defined in the same way as previously. The test prototype vehicle with 4WIS–4WID structure has all-wheel steering and therefore has more flexibility in the form of motion, such as crabbing, diagonal travel, and in situ steering. Values of deviation μ of the prototype are composed of the lateral deviation d and heading deviation θ. We can see from the works of literature that no formula was given to represent the deviation of the prototype currently. Thus, in this paper, we adopt the $\Delta\theta$, the angle between the longitudinal vehicle direction OB, and the look-ahead straight-line OS to represent the deviation of the test prototype.

$$\Delta\Theta = f(d, \theta) = \theta + \arctan(\frac{d}{LD}) \tag{3}$$

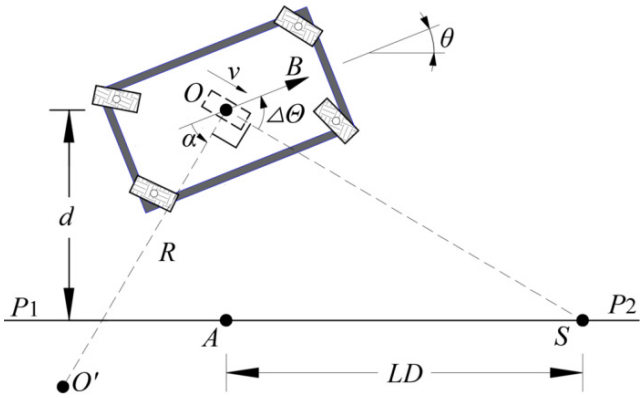

Figure 5. Schematic diagram of vehicle deviation based on the pure pursuit model.

In Equation (3), d and θ denote the lateral and heading deviation of the prototype vehicle in meters and degrees, respectively, and LD indicates the look-ahead distance in meters.

We can see that the larger the $\Delta\theta$, that is, the greater the angle between the longitudinal direction and the aiming straight line, the greater the deviation of the prototype, the closer

α is to the longitudinal direction, and the value of α is close to 0° or 180° according to the conclusion (1) in Section 2.2.2. Conversely, the smaller the $\Delta\theta$ is, the closer the α is to the axle direction; the angle is approximately 90°.

2.3. Design of Fuzzy Controller

2.3.1. Input and Output Variables

In order to obtain the appropriate steering center with a specific deviation, a two-input, two-output fuzzy controller is designed in this paper, the lateral deviation d and the heading deviation θ of the prototype vehicle between the current path and the desired path are set as the input variables, and the universe of discourse is [−1.0 m 1.0 m] and [−90° 90°], respectively. Angle α and radius R of the steering center are the output variables. The universe of discourse are [0 m 5.0 m] and [0° 90°]. When the prototype approaches the target path, the steering center's expectation of α and R should be close to 90° and 5.0 m (i.e., the prototype vehicle travels in a straight line along the desired path). If the domain of α is set to [−90° 90°] (the output of the fuzzy controller controls both left and right turns of the prototype vehicle), there will be two reasonable expectations, namely, −90° and 90°. The sudden change in the output value will lead to large fluctuations in the output of the fuzzy controller. Therefore, this paper uses the deviation $\Delta\theta$ to control the left and right turn of the prototype vehicle. When the value of $\Delta\theta$ is greater than 0°, the current prototype heading lies at the left side of the desired path, a right turn of the vehicle is necessary to minus the deviation, the momentary output α by the fuzzy controller is positive, and vice versa is a negative value.

In addition, the positive and negative signs of each variable are defined as follows: for the lateral deviation d, a positive sign is considered when the prototype vehicle locates on the left side of the desired path, and a negative when the prototype vehicle is located on the right side of the desired path. For the heading deviation θ, a positive sign is considered for anticlockwise rotation, whereas a negative convention is considered for clockwise rotation when viewed from the top. Considering the accuracy of control and the flexibility of optimization, the input variables are classified into five fuzzy subsets and defined as positive big (PB), positive small (PS), zero (O), negative small (NS), and negative big (NB). The fuzzy subsets of output variables α are defined as zero (O), small (S), medium (M), and big (B), and the fuzzy subsets of output variables $\Delta\theta$ are defined as zero (O), small (S), and big (B), respectively. A large-scale quantization level obtains higher control stability when the deviation is significant. However, a high-resolution (small-scale) quantization level is used to obtain finer adjustment of position and orientation of the prototype vehicle when the current path is close to the desired path. The triangular membership function is used for each input and output variable. The basic information of each input and each output variable is shown in Figure 6.

2.3.2. Control Rules

To increase the stability and reliability of the fuzzy controller in controlling the prototype vehicle to approach the target path, reasonable fuzzy control rules are desirable. According to the experience of experts and drivers, the following principles should be followed to generate control rules. When both lateral and heading deviations are significant, we need a smaller angle of steering (i.e., close to 0°) and a smaller steering radius to achieve a fast convergence to the desired path. However, when the deviation is slight, we need a larger steering angle (i.e., close to 90°) and a larger steering radius to fine-tune the prototype vehicle to ensure travel stability. Based on the principles mentioned above and through repeated optimization attempts, 25 control rules are designed (Table 1), and the query table is shown in Figure 7.

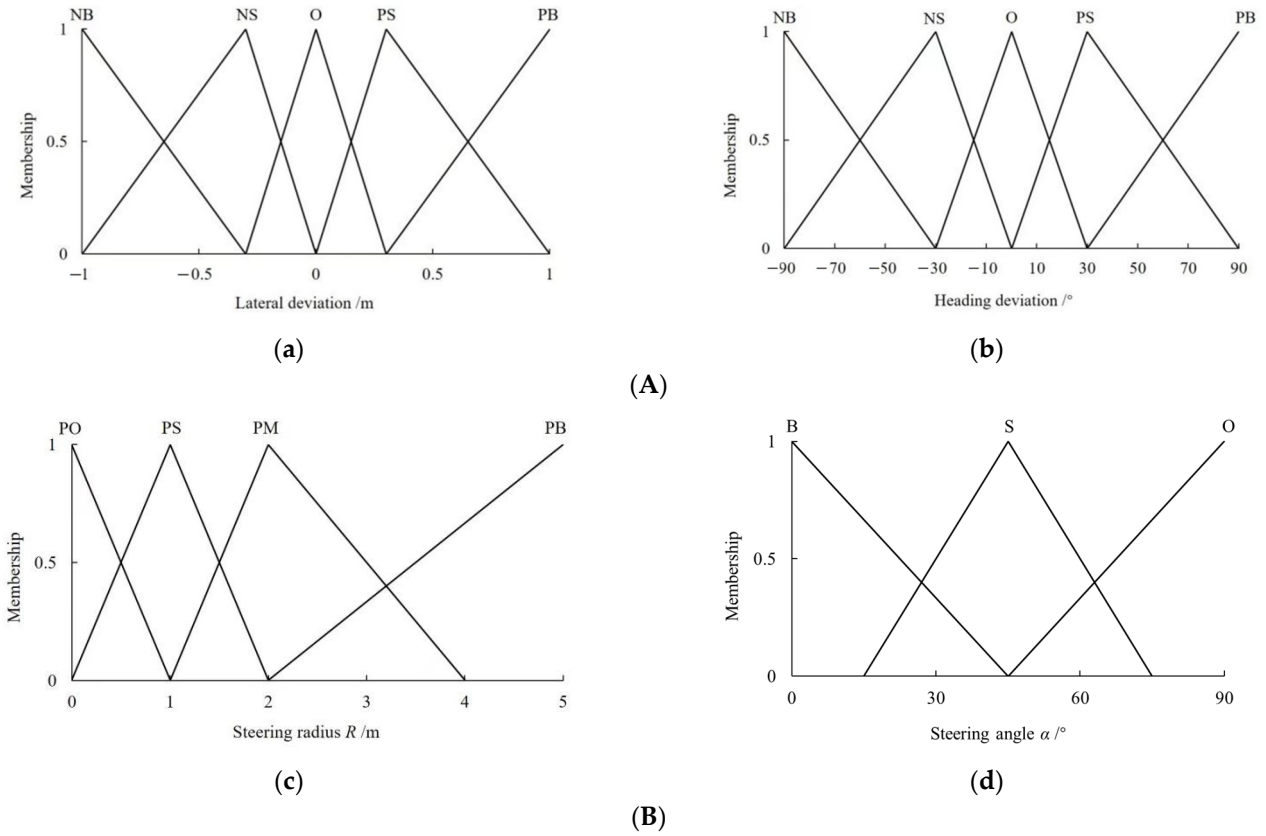

Figure 6. (**A**) Membership function of input variables. (**a**) Lateral deviation d (m), (**b**) Heading deviation θ (deg); (**B**) Membership function of output variables. (**c**) Steering radius R (m), (**d**) Steering angle α (deg).

Table 1. Fuzzy controller rules.

Variables	d	θ				
		NB	**NS**	**O**	**PS**	**PB**
α	NB	B	B	B	O	O
	NS	B	B	S	O	O
	O	B	B	O	B	B
	PS	O	O	S	B	B
	PB	O	O	B	B	B
R	NB	PS	PS	PB	PS	PS
	NS	PO	PO	PM	PO	PO
	O	PO	PO	PB	PO	PO
	PS	PO	PO	PM	PO	PO
	PB	PS	PS	PB	PS	PS

2.3.3. Validation of the Model

A comparative study of the tracking accuracy and the convergence efficiency between the traditional pure pursuit (TPP) model and the fuzzy control pursuit (FCP) model is simulated in MATLAB 2018. For the simulation, both methods adopt the identical structure of the prototype vehicle, equivalent look-ahead distance (1.5 m), the same initial state (d = 0 m, $\theta = 90^{\circ}$), and velocity (0.5 ms^{-1}). Trials of the path tracking were evaluated in terms of average deviation, steady-state deviation, stability distance, and settling time. Average deviation refers to the average value of all lateral deviations throughout the whole process of the test in millimeters. Stability distance refers to the longitudinal distance the prototype traveled when the value of lateral deviation coverage was from maximum to

within ±0.1 m for the first time (and the heading deviation converges to ±9°) in millimeters. Settling time refers to the time required for the prototype vehicle to reach the steady state from the initial state in seconds. The steady-state deviation is the mean value of the lateral deviation of all data points after the prototype vehicle reaches the steady state in millimeters. Average and steady-state deviations are critical indicators to evaluate path-tracking accuracy. Stability distance and settling time reflect the speed of the path tracking and the convergence efficiency. The simulation results are shown in Figures 8 and 9 and Table 2.

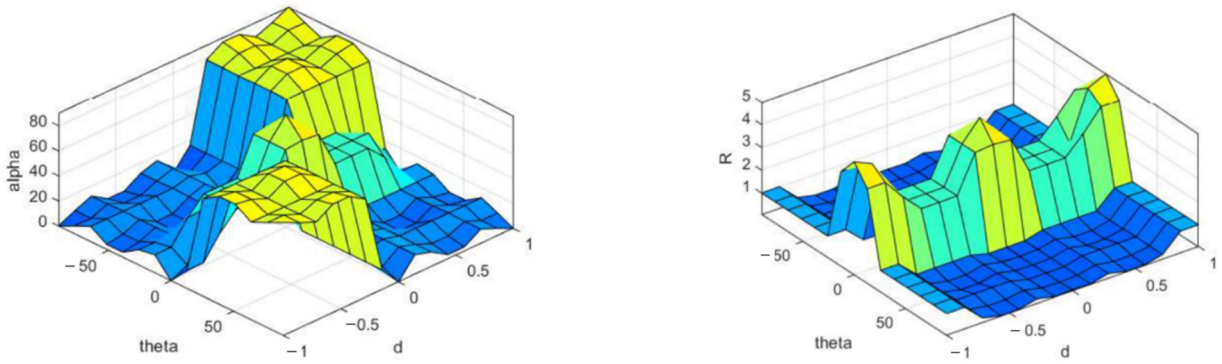

(**a**) (**b**)

Figure 7. Query table. (**a**) Query table of α, (**b**) Query table of R.

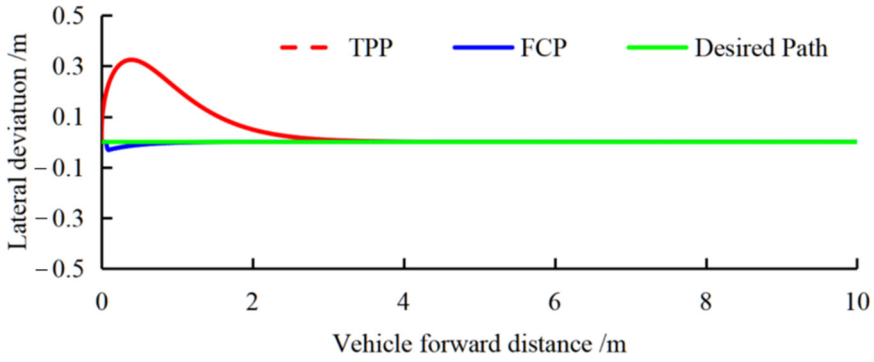

Figure 8. Comparison of the simulation trajectories of the two path-tracking methods.

Figure 8 and Table 2 shows that due to the TPP model's limitation, the steering center's steering radius is always perpendicular to the vehicle's longitudinal axis. The lateral deviation first expands and gradually decreases in the adjustment process; therefore, the average deviation value is significant. The FCP, on the other hand, obtains even higher accuracy and convergence efficiency due to the flexible position of the steering center. The d-θ diagrams of vehicle adjustment using two models are visualized in Figure 9, showing that the distance from the initial state to the desired steady state is much shorter, and the route is much straighter for FCP than TPP. Figure 10 shows the whole process of prototype vehicle adjustment in a graphic way. It can be seen that FCP takes advantage of the 4WIS–4WID structure, which makes the lateral deviation and heading deviation converge simultaneously, thus significantly improving the efficiency.

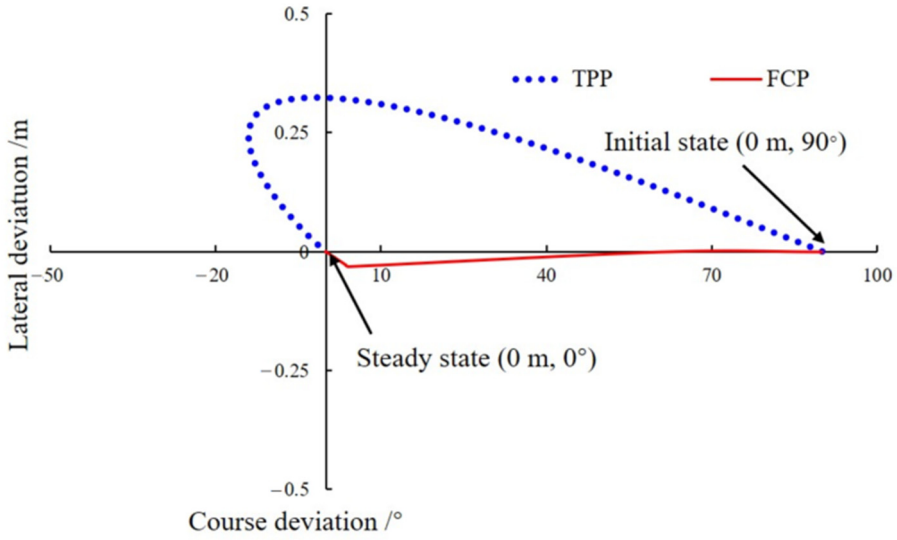

Figure 9. Comparison of the convergence efficiency (d-θ) of the two methods.

Table 2. Simulation statistics of the two methods.

Initial States	Models	Accuracy		Convergence Efficiency	
		Average Deviation/mm	Steady-State Deviation/mm	Stability Distance/mm	Settling Time/s
(0 m, 90°)	TPP	43.96	7.07	1591.85	3.7
	FCP	13.14	9.27	488.34	1.1

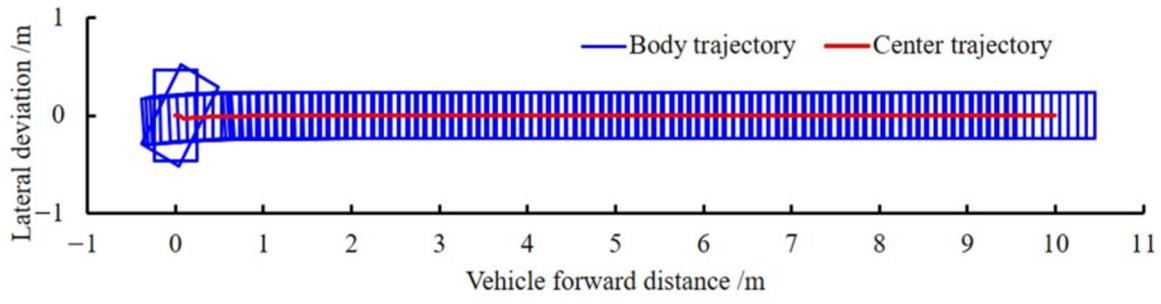

(**a**)

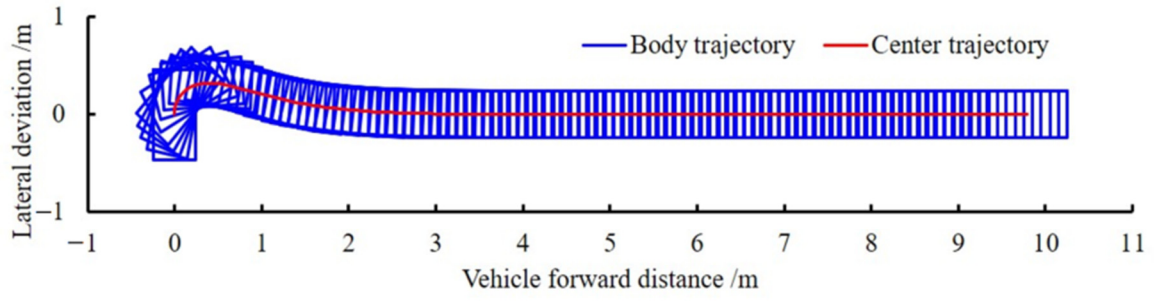

(**b**)

Figure 10. Vehicle adjustment process. (**a**) Prototype position adjustment diagram of FCP, (**b**) Prototype position adjustment diagram of TPP.

2.4. Experimental Design

To further verify the algorithm's effectiveness in this paper, the authors conducted a linear path-tracking experiment in a greenhouse at the Guan Tang farm of Zhejiang Agriculture and Forestry University from November to December 2021. The greenhouse has a size (L × W × H) of 25 m × 18 m × 3 m. It mainly grows small tomatoes and peppers, and has a path of about 3.5 m width between each cultivation bed for the test, as shown in Figure 11. The height of each UWB base station and the mobile tag from the ground is 1.6 m. The mobile tag projection point was located at the center of the 4WIS–4WID structured prototype vehicle, and the sampling frequency was 5 Hz. The location and orientation of the prototype vehicle are obtained from the gyroscope installed in the vehicle body. The prototype vehicle travels at a speed of 0.5 ms^{-1}, and the upper computer continuously records the platform's position information in the travel process.

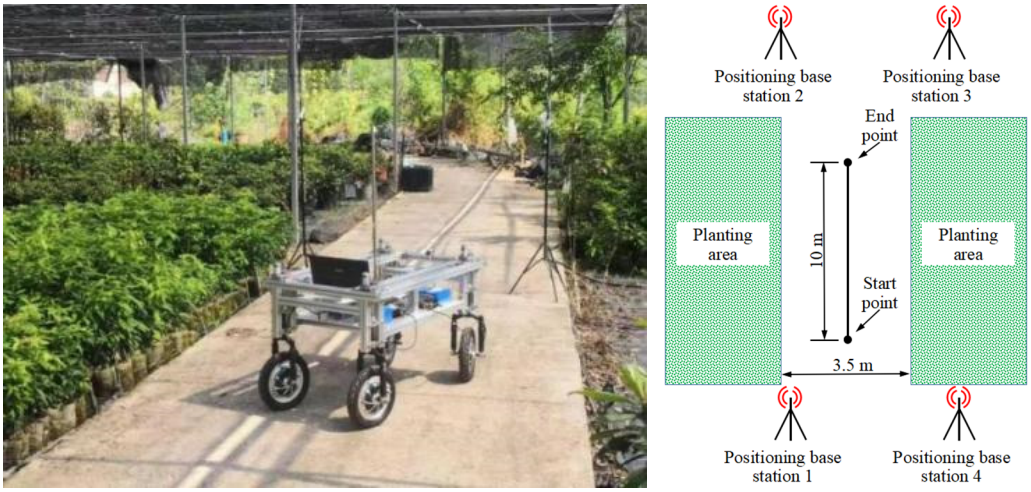

Figure 11. Test site and base station information.

3. Results and Discussion

3.1. Results of the Tests

Four linear path-tracking tests are designed under different initial states (d,θ). Variables d and θ are the same as the previous, and the initial deviation settings should be representative to make the test results credible. The initial deviation contains several limit deviations of the prototype in actual operation, namely, (1 m, 90°), (1 m, 0°), (1 m, −90°), and (0 m, 90°). The tracking accuracy and convergence efficiency evaluation indicators are the same as the above simulation test.

3.2. Analysis and Discussion

3.2.1. Path Tracking Accuracy

From Figure 12 and Table 3, it can be obtained that the average deviation of TPP under four different initial states are 620 mm, 220 mm, 277 mm, and 342 mm, respectively, which are significantly higher than 169 mm, 153 mm, 212 mm, and 38 mm of FCP. The mean value of average deviation is affected by the initial state, but the FCP path-tracking method proposed in this paper has higher accuracy than the TPP method. Nevertheless, the effect of the FCP method on tracking accuracy is more evident in the state of significant deviation. When the vehicle reaches the steady state, the steady-state deviations of FCP in four different initial states are 46 mm, 35 mm, 36 mm, and 51 mm, which are less than 100 mm and can meet the demand for high-precision path tracking in narrow environments such as greenhouses.

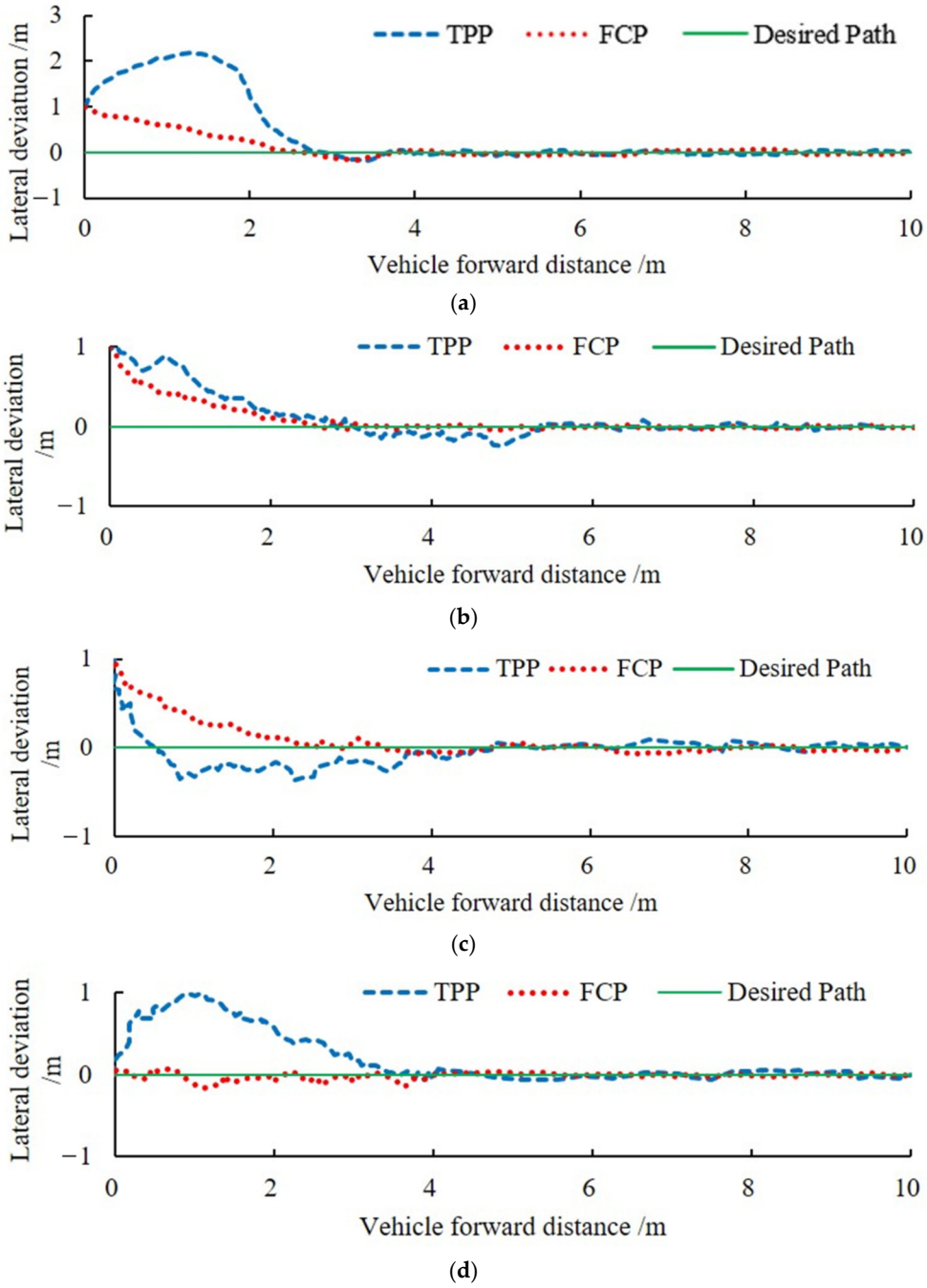

Figure 12. Comparison of tests under four initial states. (**a**) Comparison of path-tracking trajectories in the initial state (1 m, 90°), (**b**) Comparison of path-tracking trajectories in the initial state (1 m, 0°), (**c**) Comparison of path-tracking trajectories in the initial state (1 m, −90°), (**d**) Comparison of the path-tracking trajectory in the initial state (0 m, 90°).

3.2.2. Rapid Convergence

Regarding the convergence efficiency, from Figure 12 and Table 3, the stability distance of FCP under four different initial states are 2418 mm, 3052 mm, 2582 mm, and 1661 mm, significantly shorter than the corresponding stability distance of TPP, which shows that TCP has faster convergence for path tracking. The settling time of FCP is also significantly shorter than that of TPP. It can be seen from Table 2 that the stability distance is not proportional to the settling time because the settling time is highly related to the trajectory.

In contrast, the stability distance is the length of the projection line of the vehicle tracking trajectory on the *x*-axis.

Table 3. Statistics of the comparative tests.

Initial States	Tracking Model	Tracking Accuracy		Convergence Efficiency	
		Average Deviation/mm	Steady-State Deviation/mm	Stability Distance/mm	Settling Time/s
(1 m, 90°)	TPP	620	50	3914	11.7
	FCP	169	46	2418	6.2
(1 m, 0°)	TPP	220	34	5332	14.4
	FCP	153	35	3052	8.6
(1 m, −90°)	TPP	277	39	4751	12.1
	FCP	212	36	2582	6.5
(0 m, 90°)	TPP	342	48	3966	11.3
	FCP	38	51	1661	4.4

3.2.3. Effect of Initial Deviation on Stabilization Distance and Maximum Deviation

From Figure 12 and Table 3, it can also be obtained that the stability distance of the prototype vehicle reaching the steady state under four different initial states varies widely due to the inconsistency of the initial states. By Equation (3), we can see that when the initial deviation is more significant (Figure 12a,b), the time required to adjust for convergence is also more significant, the trajectory has a longer stability distance, and the maximum deviation is also the largest, and vice versa.

3.2.4. Influence of Mechanical Structure on the Quality of Path Tracking

As seen in Figure 12, the convergence trajectory of the prototype vehicle from the initial state to near the origin point in the TPP model is a tortuous spiral due to mechanical constraints, and the convergence process is relatively long. Compared with TPP, the convergence from the starting point to near the origin is much shorter in the FCP model because FCP takes full advantage of the 4WIS–4WID structure. The steering center is flexibly distributed around the vehicle's body to achieve simultaneous correction of the position and direction, which can also be seen in Figure 12.

4. Conclusions

1. Based on the 4WIS–4WID structure and fuzzy control, a tracking model for low-speed agricultural vehicles is proposed so that the steering center is not limited to the left and right extension lines of the rear axle, thus enriching the form of vehicle movement and improving the path-tracking quality and convergence efficiency.
2. In a rectangular test area 25 m long and 18 m wide with the UWB module working as a positioning system, the steady-state deviation of the prototype vehicle ranged from 41 to 79 mm for straight-line path tracking, and the average deviation of the rectangular path was 185 mm in four initial states, which makes it feasible for driving on narrow roads in the facility.
3. The mechanical structure of the prototype vehicle fits with the size of internal roads and corners of most greenhouses in China. The path-tracking method could improve the intelligent performance of vehicles used in the greenhouse, providing more feasibility for future applications such as transporting materials and conducting mechanized operations.
4. Changes in temperature and shading in the greenhouse can affect positioning accuracy. The potential wheel side-slip phenomenon will also impact path-tracking accuracy. In subsequent research, the mechanical performance of the prototype vehicle needs to be improved, and the positioning accuracy of UWB in different environments needs

to be tested. In addition, the d-θ diagram merits deepened research to achieve an ideal linear convergence effect, and also the negative correlation between the steering radius R and the integrated deviation $\Delta\theta$.

Author Contributions: Conceptualization, L.X. and L.Y.; methodology, L.X., Q.C. and L.Y.; Data curation, L.W.; software Q.C.; writing, review and editing, L.X. and L.Y. All authors have read and agreed to the published version of the manuscript.

Funding: This research was funded by Key R&D Program of Zhejiang, grant number 2022C02042.

Institutional Review Board Statement: Not applicable.

Informed Consent Statement: Not applicable.

Data Availability Statement: Not applicable.

Conflicts of Interest: The authors declare no conflict of interest. The funders had no role in the design of the study; in the collection, analyses, or interpretation of data; in the writing of the manuscript, or in the decision to publish the results.

References

1. Ahn, J.; Shin, S.; Kim, M.; Park, J. Accurate Path Tracking by Adjusting Look-Ahead Point in Pure Pursuit Method. *Int. J. Automot. Technol.* **2021**, *22*, 119–129. [CrossRef]
2. Laurense, A.V.; Jonathan, Y.; Goh, J.; Gerdes, C. Path-tracking for autonomous vehicles at the limit of friction. In Proceedings of the American Control Conference, Seattle, WA, USA, 24–26 May 2017.
3. Paden, B.; Čáp, M.; Yong, S.Z.; Yershov, D.; Frazzoli, E. A survey of motion planning and control techniques for self-driving urban vehicles. *IEEE Trans. Intell. Veh.* **2016**, *1*, 33–55. [CrossRef]
4. Kadeghe, F.; Wesley, P.; Edward, B.; Li, C.; Glen, R. Autonomous navigation of a center-articulated and Hydrostatic transmission rover using a modified pure pursuit algorithm in a cotton field. *Sensors* **2020**, *20*, 4412. [CrossRef] [PubMed]
5. Rains, G.C.; Faircloth, A.G.; Thai, C.; Raper, R.L. Evaluation of a simple pure pursuit path-following algorithm for an autonomous, articulated-steer vehicle. *Appl. Eng. Agric.* **2014**, *30*, 367–374.
6. DeSantis, R.M.; Bourgeot, J.M.; Todeschi, J.N.; Hurteau, R. Path-tracking for tractor-trailers with hitching of both the on-axle and the off-axle kind. In Proceedings of the IEEE Internatinal Symposium on Intelligent Control, Vancouver, BC, Canada, 30 October 2002; pp. 206–211.
7. Ferentinos, K.P.; Arvanitis, K.G.; Kyriakopoulos, K.; Sigrimis, N. Heuristic Motion Planning for Autonomous Agricultural Vehicles. In *Bio-Robotics, Information Technology and Intelligent Control for Bioproduction Systems*; Department of Agricultural and Biological Engineering Cornell University: Ithaca, NY, USA, 2001; p. 14853.
8. Wang, L.; Liu, M. Path Tracking Control for Autonomous Harvesting Robots Based on Improved Double Arc Path Planning Algorithm. *J. Intell. Robot. Syst.* **2020**, *10*, 899–909. [CrossRef]
9. Zhang, W.; Gai, J.; Zhang, Z.; Tang, L.; Ding, Y. Double-dqn based path smoothing and tracking control method for robotic vehicle navigation. *Comput. Electron. Agric.* **2019**, *166*, 104985. [CrossRef]
10. Xu, F.; Liu, X.; Chen, W.; Zhou, C. Dynamic switch control of steering modes for four wheel independent steering rescue vehicle. *IEEE Access* **2019**, *7*, 135595. [CrossRef]
11. Guo, L.; Yang, B.; Ye, J. Enhanced Cyber-physical Security of Steering Stability Control System for Four-Wheel Independent Drive Electric Vehicles. In Proceedings of the IEEE Transportation Electrification Conference and Expo, Nanning, China, 1 June 2020.
12. Liu, H.; Yan, S.; Shen, Y.; Li, C.; Zhang, Y.; Hussain, F. Model predictive control system based on direct yaw moment control for 4WID self-steering agriculture vehicle. *Int. J. Agric. Biol. Eng.* **2021**, *14*, 175–181. [CrossRef]
13. Ma, H.; Li, C.; Wang, Z. Direct Yaw-Moment Control Based on Fuzzy Logic of Four Wheel Drive Vehicle under the Cross Wind. *Energy Procedia* **2017**, *105*, 2310–2316.
14. Liu, J.; Geng, L.; Wang, K.; Liu, W.; Liu, J.; Wang, K.; Liu, W. Research on 4WS-DS Control Strategy of Electric Wheel Vehicle. In *Society of Photo-Optical Instrumentation Engineers (SPIE) Conference Series*; SPIE: Bellingham, WA, USA, 2021.
15. Muhammad, A.K.; Muhammad, F.A.; Ejaz, A.; Iljoong, Y. Robust Differential Steering Control System for an Independent Four Wheel Drive Electric Vehicle. *Int. J. Automot. Technol.* **2019**, *20*, 87–97.
16. Yim, S. Integrated Chassis Control With Four-Wheel Independent Steering Under Constraint on Front Slip Angles. *IEEE Access* **2021**, *9*, 10338–10347. [CrossRef]
17. Jing, L.; Zhang, Y.; Shen, Y.; He, S.; Liu, H.; Cui, Y. Adaptative Trajectory Tracking Control of 4WID High Clearance Unmanned Sprayer. *Trans. Chin. Soc. Agric. Mach.* **2021**, *52*, 408–416.

18. Zhang, J.; Chen, D.; Wang, S.; Hu, X.; Wang, D. Design and experiment of four-wheel independent steering driving and control system for agricultural wheeled robot. *Trans. Chin. Soc. Agric. Eng.* **2015**, *31*, 8.
19. Coulter, R.C. *Implementation of the Pure Pursuit Path Tracking Algorithm*; Carnegie-Mellon University, The Robotics Institute: Pittsburgh, PA, USA, 1992.